Bredow, E., Steinberger, B., Gassmöller, R., Dannberg, J. (2017): How plume-ridge interaction shapes the crustal thickness pattern of the Réunion hotspot track. - *Geochemistry Geophysics Geosystems (G3)*, *18*, 8, pp. 2930—2948.

DOI: http://doi.org/10.1002/2017GC006875

AGU PUBLICATIONS

Geochemistry, Geophysics, Geosystems

RESEARCH ARTICLE
10.1002/2017GC006875

How plume-ridge interaction shapes the crustal thickness pattern of the Réunion hotspot track

Eva Bredow[1], Bernhard Steinberger[1,2], Rene Gassmöller[3], and Juliane Dannberg[3,4]

[1]GFZ German Research Centre for Geosciences, Potsdam, Germany, [2]Centre for Earth Evolution and Dynamics, University of Oslo, Oslo, Norway, [3]Department of Mathematics, Colorado State University, Fort Collins, Colorado, USA, [4]Department of Mathematics, Texas A&M University, College Station, Texas, USA

Key Points:
- Réunion plume model predicts crustal thickness pattern comparable to actual hotspot track
- Gap between Maldives and Chagos generated due to ridge geometry and plume-ridge interaction
- Rodrigues Ridge formed by sublithospheric flow channel between plume and Central Indian Ridge

Supporting Information:
- Supporting Information S1
- Movie S1
- Data Set S1

Correspondence to:
E. Bredow,
eva.bredow@gfz-potsdam.de

Citation:
Bredow, E., B. Steinberger, R. Gassmöller, and J. Dannberg (2017), How plume-ridge interaction shapes the crustal thickness pattern of the Réunion hotspot track, *Geochem. Geophys. Geosyst.*, *18*, 2930–2948, doi:10.1002/2017GC006875.

Received 15 FEB 2017
Accepted 27 JUN 2017
Accepted article online 15 JUL 2017
Published online 9 AUG 2017
Corrected 5 SEP 2017

This article was corrected on 5 SEP 2017. See the end of the full text for details.

Abstract The Réunion mantle plume has shaped a large area of the Earth's surface over the past 65 million years: from the Deccan Traps in India along the hotspot track comprising the island chains of the Laccadives, Maldives, and Chagos Bank on the Indian plate and the Mascarene Plateau on the African plate up to the currently active volcanism at La Réunion Island. This study addresses the question how the Réunion plume, especially in interaction with the Central Indian Ridge, created the complex crustal thickness pattern of the hotspot track. For this purpose, the mantle convection code ASPECT was used to design three-dimensional numerical models, which consider the specific location of the plume underneath moving plates and surrounded by large-scale mantle flow. The results show the crustal thickness pattern produced by the plume, which altogether agrees well with topographic maps. Especially two features are consistently reproduced by the models: the distinctive gap in the hotspot track between the Maldives and Chagos is created by the combination of the ridge geometry and plume-ridge interaction; and the Rodrigues Ridge, a narrow crustal structure which connects the hotspot track and the Central Indian Ridge, appears as the surface expression of a long-distance sublithospheric flow channel. This study therefore provides further insight how small-scale surface features are generated by the complex interplay between mantle and lithospheric processes.

1. Introduction

1.1. Geodynamic History of the Réunion Plume

The mantle plume currently inducing volcanic activities on La Réunion Island in the western Indian Ocean (Figure 1) has continuously affected the surface of the Earth over the past 65.5 Myr [e.g., *Duncan*, 1990; *Courtillot et al*., 2003; *Hofmann et al*., 2000; *Schoene et al*., 2015]. When the ascending plume head arrived at the base of the lithosphere and induced partial melting, the subsequent surface volcanism created the Deccan Traps in India, a Large Igneous Province (LIP) that marks the spatial and temporal beginning of the Réunion hotspot track [*Richards et al*., 1989]. Most of these continental flood basalts were erupted in less than 1 Myr [*Courtillot et al*., 1986, 1988] and this relatively short period of vigorous magmatic activity is associated with the mass extinction at the Cretaceous/Tertiary boundary [*Courtillot and Renne*, 2003]. Between 67 and 51 Ma, India moved with anomalously high plate velocities of up to 16 cm/yr, which *van Hinsbergen et al*. [2011] partly attributed to the Réunion plume, since the plume head impinging on the lithosphere may have acted as a lubricant to accelerate the plate. *Cande and Stegman* [2011] proposed the rapid movement of the Indian plate to be caused only by the pushing force of the rising plume head. The Indian plate and later the African plate moved above the relatively fixed plume tail and created the Réunion hotspot track [*Duncan and Hargraves*, 1990; *Duncan and Richards*, 1991], a linear chain of age-progressive islands, seamounts, and plateaus (Figure 1). From its initiation at the Deccan Traps, the hotspot track can be followed southward along the island chains of the Laccadives, the Maldives and across a rather uncommon gap along the Chagos Bank on the Indian and Australian plate and southwestward along the Mascarene Plateau including the Mascarene Islands Mauritius and Réunion on the African plate [*Duncan*, 1990]. Seafloor-spreading at the Central Indian Ridge has split the once continuous hotspot track between the Chagos Bank and the Northern Mascarene Plateau [*McKenzie and Sclater*, 1971]. Today, the frequent eruptions of the Piton de la Fournaise at La Réunion represent the surface activities of the plume [*Richards et al*., 1989].

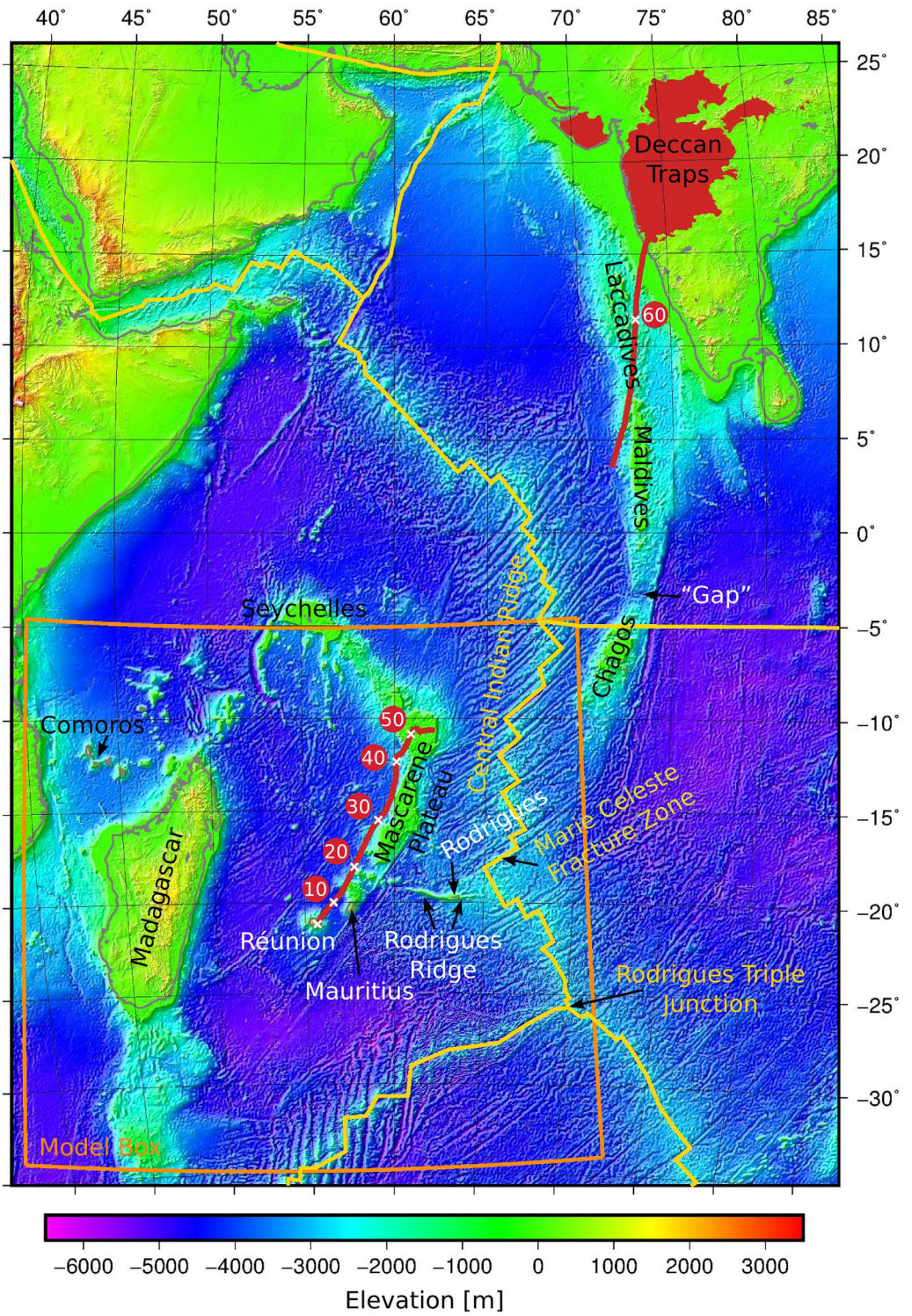

Figure 1. Topographic map of the northwestern Indian Ocean showing the entire hotspot track from the Deccan Traps in India to the currently active plume position at Réunion Island. The red line shows the predicted hotspot track after *Torsvik et al*. [2013] with plume positions (in Ma), the extent of the model box is depicted by the orange outline and plate boundaries are shown as yellow lines.

An unusual feature associated with the Réunion hotspot is the third Mascarene Island Rodrigues (Figure 1), situated above a narrow volcanic ridge that seems to connect a recent part of the hotspot track with the closest segment of the Central Indian Ridge. Already *Morgan* [1978] interpreted the Rodrigues Ridge as the

result of a sublithospheric flow channel created by long-distance plume-ridge interaction. Even more exceptional for a hotspot track is the hypothesis of *Torsvik et al*. [2013] and *Ashwal et al*. [2017], who analyzed the ages of Mauritian zircons from basaltic beach sand samples and zircons recovered from trachytic rocks, respectively, and concluded that Mauritius and the Mascarene Plateau overlie and conceal a Precambrian microcontinent underneath the hotspot track.

1.2. Deep Origin of the Réunion Plume

Apart from the LIP, the hotspot track and the still active volcanism, several additional characteristics indicate that the origin of the Réunion hotspot is a deep plume rising from the lowermost mantle [e.g., *Morgan*, 1971; *Courtillot et al*., 2003]. A broad topographic swell around the present-day hotspot has been noted by *Crough* [1983] and *Davies* [1988]. The Réunion plume is considered sufficiently buoyant to ascend through the entire mantle and cause volcanic activity on the surface [*Sleep*, 1990; *Courtillot et al*., 2003]. Geochemical observations report a high isotopic $^{3}He/^{4}He$ ratio of volcanic rocks from La Réunion Island that differs from typical values of mid-ocean ridge basalt (MORB) [*Farley and Neroda*, 1998; *Courtillot et al*., 2003]. Around 20°S along the Central Indian Ridge, a geochemical anomaly has been associated with plume-ridge interaction by *Mahoney et al*. [1989], *Schilling* [1991], *Nauret et al*. [2006], and *Füri et al*. [2011]. Furthermore, the reconstructed eruption site of the Deccan Traps as well as the present-day hotspot position are located almost exactly above the margin of the African Large Low Shear Velocity Province (LLSVP) [*Garnero et al*., 2007], which is considered to act as a plume generation zone at the core-mantle boundary [*Torsvik et al*., 2006; *Burke et al*., 2008]. Seismic evidence of a deep Réunion plume has been implied by previous global tomography studies [*Montelli et al*., 2004, 2006; *French and Romanowicz*, 2015] and is currently investigated by the French-German RHUM-RUM project (Réunion Hotspot and Upper Mantle—Réunions Unterer Mantel), the largest seismological experiment to image a deep oceanic mantle plume so far [*Barruol and Sigloch*, 2013].

1.3. Motivation for Modeling the Réunion Plume

The main purpose of this study, which is part of the RHUM-RUM project, is to investigate how the Réunion plume, especially in interaction with the Central Indian Ridge, created the hotspot track, i.e., if the current crustal thickness pattern in the Indian Ocean may be explained by a numerical model with a plume. Apart from the large-scale pattern, two smaller features and their origins are particularly interesting: first, it remains unclear which mechanisms in this specific geographic setting formed the gap between the Maldives and the Chagos Bank and second, the Rodrigues Ridge was suggested to be the surface expression of a sublithosphere flow channel by *Morgan* [1978]. However, there is no quantitative analysis so far that shows which dynamic processes might lead to melt production along the Rodrigues Ridge and thus support the feasibility of Morgan's hypothesis.

2. Model Setup

2.1. Numerical Model

The model setup for studying the Réunion plume is based on the procedure described in *Gassmöller et al*. [2016], which presented several software extensions for ASPECT in order to focus on a specific mantle plume—in that case the Tristan da Cunha plume in the South Atlantic. ASPECT (Advanced Solver for Problems in Earth's ConvecTion) is an open-source mantle convection code using finite elements and adaptive meshes [*Kronbichler et al*., 2012; *Bangerth et al*., 2017]. The extended ASPECT version of *Gassmöller et al*. [2016] was modified as necessary for creating a regional numerical model of the upper part of the Réunion plume.

The model domain is a three-dimensional Cartesian box, extending 3300 km × 3300 km horizontally and 660 km vertically (see Figure 2a). To cover the entire geodynamic development of the Réunion plume, the time evolution starts at 80 Ma. The boundary conditions for the box are chosen in such a way that the model explicitly represents the region around the Réunion plume: on the top boundary and the uppermost 200 km of the side boundaries, reconstructed tectonic plate velocities are prescribed to simulate plate motions. In this simplified approach based on the reference frame of *Doubrovine et al*. [2012], the velocities of each plate are kept constant for 10 Myr intervals, but the position of the mid-ocean ridges are updated in 1 Myr intervals (interpolated from the plate reconstructions of *Torsvik et al*. [2010]).

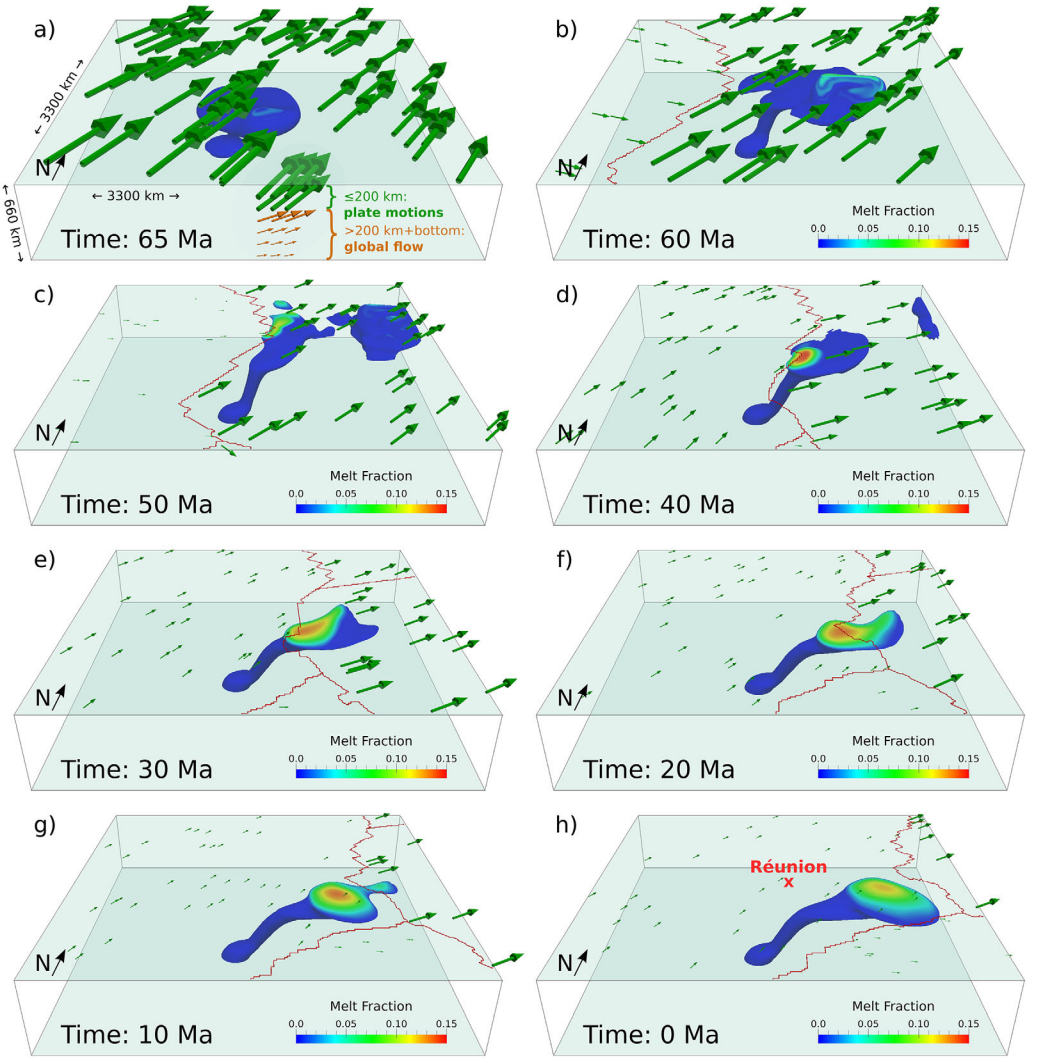

Figure 2. Development of the reference model: plume and plume-ridge interaction over time. The plume is represented by the $\Delta T = 100$ K isosurface and colored according to the melt fraction. Mid-ocean ridges are marked as red lines, the plate velocities are depicted by green arrows. (a) Additionally illustrates the velocity side boundary conditions: orange arrows show the global flow on the same scale as the plate motions. (h) Represents the present-day state and shows the position of Réunion Island.

Below 200 km at the side boundaries and at the bottom of the box, time-dependent global flow velocities are prescribed to take into account the large-scale mantle circulation. The mantle flow velocities are derived from a global mantle convection model with a lower resolution (an update of *Doubrovine et al.* [2012]), which derives the present-day mantle flow from a density model based on seismic tomography, a surface boundary condition in agreement with plate motions and the radial viscosity structure of *Steinberger and Calderwood* [2006], whereas the mantle flow in the past is computed by backward-advecting density anomalies with global plate motions. The global flow on the edges of the model box does not exceed a few cm/yr. Its direction is dominated by the large-scale convection cell from the upward flow above the African LLSVP southwest of the box toward the downward flow at the Sunda Trench northeast of the box.

At 200 km depth at the side boundaries, approximately corresponding to the lithosphere-asthenosphere boundary, the plate velocities, and global flow velocities are interpolated to ensure a smooth transition between the different velocity values. More details about the boundary conditions and their conversion into Cartesian coordinates suitable for the box geometry can be found in *Gassmöller et al.* [2016].

Regarding the hotspot motion model, the plume position in the coarser global model is tracked over time at the appropriate depth of 660 km and used as time-dependent plume inflow position at the bottom of

the box in order to set up a reference model where the hotspot surface position is approximately matched. The inflow position moves relatively slow: approximately 150 km eastward and 200 km southward over 67 Myr.

The initial temperature profile of the model is adiabatic with a potential surface temperature of 1613 K and a nonadiabatic cold lithospheric layer on top. The base of the lithosphere is considered to be represented by the 1613 K isotherm, which initially varies between 10 and 210 km depth in the reference model (and between 10 and 300 km depth in model variation LithThickNew). The initial lithosphere thickness is converted into half-space cooling ages and temperature profiles to be prescribed as initial temperature condition and later as boundary condition (updated in 1 Myr intervals) in ASPECT (see section 2.2). Note that except for the initial state of the model, the lithosphere thickness is only imposed on the boundaries—inside the model domain, the lithosphere thickness evolves fully dynamically. The viscosity depends on the temperature and considers lateral variations besides the radial structure of *Steinberger and Calderwood* [2006] (see section 2.3).

The occurrence of temperature-dependent and pressure-dependent melting is calculated based on the parametrization for batch melting of anhydrous peridotite [*Katz et al*., 2003]. As a postprocessing step, the melt generated in each time step is instantly extracted, accumulated at the surface and moved along with the tectonic plate motions (instant melt extraction method of *Gassmöller et al*. [2016]). This procedure assumes that melt ascends through channels and dikes in the lithosphere and produces magmatic crust vertically above the origin of the melt. Note that lateral melt motion is neglected since the ascent through channels and dikes occurs much faster than motion in the mantle. The final result shows the present-day crustal thickness pattern of the Réunion hotspot track (see section 3.2).

Every model run is computed twice, using the net mass flux from the first model run to correct the velocity boundary conditions used in the second computation, to assure that there is no net mass influx or outflux. This compensates in particular for the plume inflow. Only the second computation is presented as a result and interpreted. The boundary velocity correction is equally distributed over the asthenosphere (below 200 km depth) of the four side boundaries and except for the time of the plume head inflow, the corrections do not exceed 0.3 cm/yr.

Since every model has to be computed twice, each run taking about 10 h on 768 processors, each variation of the model requires approximately 15,000 core hours of computing time and has about 12 million degrees of freedom. The adaptive mesh refinement enables a better resolution of the plume and the lithosphere, where melting occurs. The smallest mesh cells in the uppermost 200 km have a size of 10.3 km.

2.2. Lithosphere Thickness Values as Initial and Boundary Conditions

The geodynamic processes in the Western Indian Ocean are challenging for a localized model setup. At the start time of the model, the top of the box is not completely covered by continents, therefore an initially homogeneous lithosphere thickness is rather unrealistic. Another intricacy is caused by the plate motions on top of the box. Since they do not symmetrically diverge from the Central Indian Ridge, most of the lithosphere thickness is controlled by the boundary conditions instead of being self-consistently generated by the model. Therefore, the global lithospheric thickness model of *Steinberger* [2016] (or model LITHO1.0 of *Pasyanos et al*. [2014] with a formal lateral resolution of 1° in modified model LithThickNew) was used to initialize and prescribe the thermal structure at the model boundaries and the time of model initiation according to the backward rotated positions of oceans and continents. (Note that *Steinberger* [2016] uses a different isotherm to define lithosphere thickness.) The backward-rotation was carried out using absolute plate motions from *Doubrovine et al*. [2012] and relative rotations from *Torsvik et al*. [2010]. In the oceans, the lithosphere thickness is derived from the Earthbyte ocean floor age (version 3.6 of *Müller et al*. [2008]), i.e., the present-day age grid is backward-rotated and converted to a half-space cooling temperature profile using a thermal diffusivity value $\kappa = 8 \times 10^{-7} m^2 s^{-1}$ (more details available in supporting information Text S4 in *Gassmöller et al*. [2016]).

Note that the microcontinent described by *Torsvik et al*. [2013] and *Ashwal et al*. [2017] is not considered in these boundary conditions, since the age grid of *Müller et al*. [2008] (with a formal resolution of 6 arc min) differentiates only between continents and oceans and apart from the Seychelles, the entire area of the microcontinent is classified as ocean.

2.3. Dehydration Rheology and Depletion Buoyancy

When rising mantle material crosses the solidus and starts to melt, water is extracted and this dehydration effect leads to an immediate viscosity increase that stiffens the lithosphere and suppresses buoyancy-driven flow, lowering the melt production rate. Including a dehydration rheology is therefore a mechanism known to reduce the melting rate and thus produce thinner crust [*Ito et al*., 1999; *Howell et al*., 2014]. Due to the neglect of this process, *Gassmöller et al*. [2016] report very high crustal thickness values in some small regions of their result, which inspired the incorporation of a dehydration rheology for the Réunion model.

The numerical implementation of this sudden viscosity jump is achieved by a preexponential factor A controlling the viscosity. While *Ito et al*. [1999] chose the constant factor of $A = 1$ below and $A = 50$ above the dry solidus, *Howell et al*. [2014] used a term depending on the percentage of water dissolved in the solid mantle material: $A=(C/C_0)^{-1}$ describes the dependence on the water concentration in the solid, C, proportionally to the water dissolved at the beginning, C_0, if a dehydration effect is desired. The equivalent dehydration prefactor after *Katz et al*. [2003] yields

$$A=\left(\frac{C}{C_0}\right)^{-1}=\frac{D_{H_2O}+F(1-D_{H_2O})}{D_{H_2O}} \tag{1}$$

where D_{H_2O} is a bulk partitioning coefficient with a value of 0.01 and F is the current weight fraction of melt or degree of depletion. In the absence of melt, i.e., $F = 0$, the viscosity should not be altered by the dehydration prefactor, therefore the denominator is D_{H_2O}. The viscosity finally simulated in the Réunion plume models combines the dehydration rheology from *Howell et al*. [2014] and a slightly modified version of the temperature-dependence and depth-dependence in *Steinberger and Calderwood* [2006] and thus is a product of the dehydration prefactor, the radial viscosity $\eta_r(z)$ and the lateral viscosity:

$$\eta(z,T)=\frac{D_{H_2O}+F(1-D_{H_2O})}{D_{H_2O}}\cdot\eta_r(z)\cdot\exp\left(-\frac{(E+pV)(T-T_{adi}(z))}{nRTT_{adi}(z)}\right) \tag{2}$$

where $T_{adi}(z)$ is the depth-dependent adiabatic temperature, n is the stress exponent, and R is the universal gas constant.

Further, the depth-dependent activation enthalpy profile $H(z)$ of *Steinberger and Calderwood* [2006] was replaced by the term $E + pV$ with the activation energy $E=3.75\times10^5$ J/mol and the activation volume $V=6\times10^{-6}$ J/(mol Pa) and $n = 1$ after *Hirth and Kohlstedt* [2003]. This rheology leads to more realistic viscosities, because only considering the temperature dependence of viscosity from *Steinberger and Calderwood* [2006] but disregarding the effect that higher strain rates inside a plume yield lower viscosities would underestimate the effective lateral viscosity variations [*Christensen*, 1983]. The viscosity contrast between plume and ambient mantle is increased from a factor of 4 before the change to a range of 6–20 afterward.

Additionally, the density calculation in this study includes a depletion density decrease of up to 15 kg/m^3, which increases the effective buoyancy when melt is extracted [e.g., *Dupeyrat et al*., 1995; *Manglik and Christensen*, 1997; *Ribe and Christensen*, 1999].

2.4. Reference Model and Parameter Variations

The parameters for the reference model were chosen in accordance with published values and varied in a series of additional simulations in order to constrain the influence of each parameter on the predicted pattern and thickness of the hotspot track (see Table 1 for an overview of the model setups).

The plume head inflow at the bottom of the box is simulated by a spherical velocity anomaly (a circular inflow area, which changes its radius over time) with an excess temperature ΔT, radius R, and a vertical inflow velocity v. The parameters of the plume head in the reference model are $\Delta T_{head}=$ 300 K, $R_{head}=$ 250 km, and $v_{head}=$ 20 cm/yr corresponding to the values of *Gassmöller et al*. [2016], based on the argument that the magma volumes of the Paraná-Etendeka flood basalts and the Deccan Traps are similar. More specifically, published volumes for the Deccan Traps range from 1×10^6 km^3 to $>2\times10^6$ km^3 [*Officer et al*., 1987; *Jay and Widdowson*, 2008; *Turcotte and Schubert*, 2002; *Richards et al*., 1989; *Todal and Eldholm*, 1998; *Courtillot et al*., 2003]. At 68 Ma, the plume head reaches the boundary between lower and upper mantle and enters the reference model. It continues ascending up to the base of the lithosphere and the first melt is

Table 1. Model Setups

	Excess Temperature	Inflow Velocity	Inflow Radius	Buoyancy Flux
Model	ΔT_{tail} (K)	v_{tail} (cm/yr)	R_{tail} (km)	B_{tail} (kg/s)
Reference	250	6.0	140	1250–1500
DeltaT200	200	4.8	140	700–850
DeltaT300	300	7.2	140	2100–2450
Flux950	250	5.6	120	850–1050
Flux1900	250	6.3	160	1650–2050
FixedPlume	Plume inflow position fixed at its initial position below Deccan Traps			
PlumePosVar5	Hotspot motion starts further north and ends further west			
PlumePosVar9	Hotspot moves westward from its initial position below Deccan Traps			
LithThickNew	Lithosphere thickness based on *Pasyanos et al.* [2014]			
HomLith	Homogeneous lithosphere thickness as initial and boundary conditions			
NoGlobalFlow	Without global flow (pure plume buoyancy flux = 1150 kg/s)			
NoDehyd	No dehydration rheology			
NoDepl	No depletion buoyancy			
DefaultVisc	Viscosity contrast of *Gassmöller et al.* [2016]			
+ respective NoPlume models in order to extract the contribution of the plume				

generated at 66 Ma, which represents the first volcanic activities at the Deccan Traps site. This timing agrees with geological age studies [e.g., *Courtillot et al.*, 2003].

The plume head is followed by the plume tail, prescribed as an inflow with a Gaussian circular temperature and velocity distribution at the bottom of the box. Estimations of the excess temperature of the Réunion plume tail ΔT_{tail} cover a wide range of values between 174 and 240 K [*Schilling*, 1991; *Putirka*, 2008; *Turcotte and Schubert*, 2002; *Sleep*, 1990; *Herzberg and Gazel*, 2009]. The value chosen for the plume inflow at the bottom of the reference model is 250 K and varied between 200 and 300 K in model DeltaT200 and DeltaT300, respectively. These values exceed the published estimates to account for the heat loss of approximately 40 K due to adiabatic cooling and thermal conduction while the plume material rises from the inflow depth of 660 km to the depth of the melting region. Consequently, the plume excess temperature upon melting is approximately 210 K and within the range of published estimates. In the reference model, $v_{tail} = 6$ cm/yr and $R_{tail} = 140$ km.

The plume buoyancy flux can be determined as $B_{tail} = \pi \cdot R_{tail}^2 \cdot v_{tail} \cdot (\rho_{mantle} - \rho_{tail})$, where ρ_{mantle} is the density of the ambient mantle and ρ_{tail} is the plume density [*Turcotte and Schubert*, 2002]. Estimated values for the Réunion plume tail are distributed over a broad spectrum from 900 to 1900 kg/s [*Davies*, 1988; *Schilling*, 1991; *Turcotte and Schubert*, 2002; *Sleep*, 1990]. In the reference model, the buoyancy flux ranges from 1250 to 1500 kg/s. It varies over time, because the global flow velocities at the bottom boundary interfere with the plume inflow velocity. The pure plume buoyancy flux can be measured in the model without global flow and yields 1150 kg/s. The variation of B_{tail} for other model configurations is achieved indirectly by changing v_{tail} and R_{tail} while ΔT_{tail} remains constant and yields ranges between 850 and 1050 kg/s (model Flux950) and 1650 and 2050 kg/s (model Flux1900).

Further parameters that were varied to examine their respective effects are the hotspot motion model (manually varied to a fixed or differently moving plume inflow position), the lithosphere thickness values used as initial and boundary conditions (using different reconstructions or a simplified constant lithosphere thickness), the global flow, the dehydration rheology, the depletion buoyancy, and the implemented viscosity contrast.

3. Results

3.1. Model Development

Figures 2 and 3 illustrate the chronological development of the plume in the reference model. While Figure 2 shows the plume-ridge interaction in relation to the plate motions prescribed as top boundary conditions, Figure 3 illustrates how the plume interacts with the relief of the lithospheric base. For an animated view see supporting information Movie S1; Figures S1 and S2 show corresponding figures of model NoGlobalFlow.

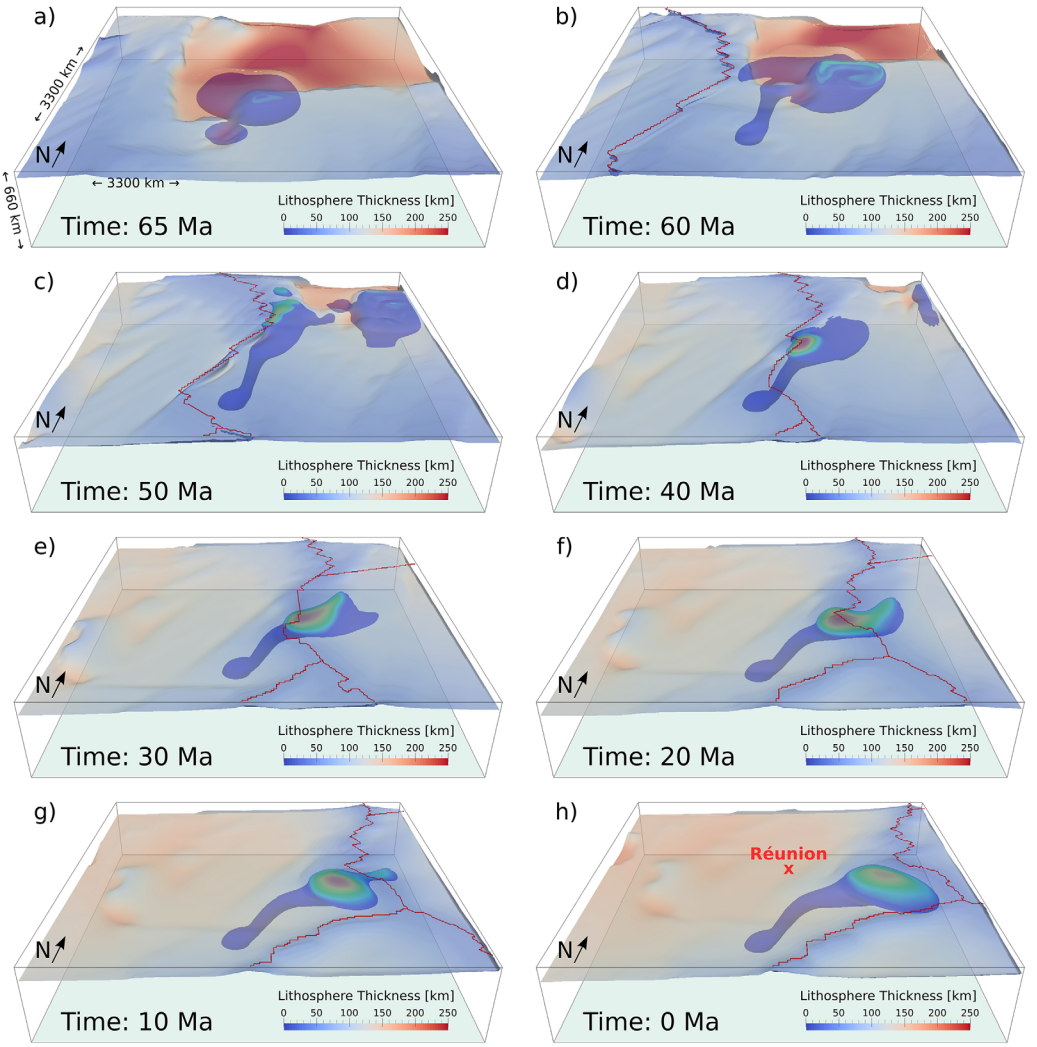

Figure 3. Development of the reference model: lithospheric thickness evolution and plume-ridge interaction over time. The plume is colored according to the melt fraction (as in Figure 2), mid-ocean ridges are marked as red lines and the base of the lithosphere is color-coded according to the depth. (h) Represents the present-day state and shows the position of Réunion Island.

At 65 Ma, the Indian plate is moving extremely fast with about 16 cm/yr (Figure 2a), while the plume head reaches the base of the thick continental lithosphere of India (Figure 3a), underneath the reconstructed site of the Deccan Traps. The onset of melting illustrates the beginning volcanic activities of the LIP, which agrees temporally with identified geological ages [e.g., *Courtillot et al.*, 2003]. However, melting does not occur at the location of the Deccan Traps, because the plume material flows southeastward (despite the northeastward plate motions and global flow) toward thinner oceanic lithosphere before it starts to melt, a process known as upside-down drainage [*Sleep*, 1997].

Over the following 5 Myr, the bulk of the asymmetrically shaped Deccan Traps southeast of the Indian continent is generated in the model (Figures 2b and 3b). Geological studies concluded that most of the LIP was formed within 1 Myr [*Courtillot et al.*, 1986, 1988], but this process takes longer in the simulation. These slightly longer time scales are likely caused by the assumption of a pure diffusion creep rheology—dislocation creep would lower the viscosity within the plume and accelerate its spreading below the lithosphere—and mechanically treating the material as solid, neglecting the thinning of the lithosphere that would be induced by the transport and freezing of melt [*Sobolev et al.*, 2011]. Note how the initially vertical plume tail starts to be tilted toward the northeast, due to the plate motions and especially the global flow (see supporting information Figures S1 and S2 for a comparison to the model without global flow). In accordance with the plate motions and plate boundaries of *Doubrovine et al.* [2012] and *Torsvik et al.* [2010], the mid-

ocean ridge between the Indian and the African plate appears in the model domain at 61 Ma and approaches the plume from the west afterward.

At 50 Ma, the Indian plate has slowed down from the record velocities, but is still moving northeastward (Figure 2c), causing India and the Deccan Traps to leave the model domain. The plume is now in the vicinity of the Central Indian Ridge and gets captured. Plume-ridge interaction increases the melt fraction and initiates the beginning of the on-ridge hotspot track. Note that the lithospheric thickness close to the ridge is self-consistently determined by the model (Figure 3c), while boundary conditions determine the thickness in the west and south.

At 40 Ma, major plume-ridge interaction takes place with the highest melt fraction of 14.5% above the plume (Figures 2d and 3d). And while the Central Indian Ridge continues to move northeastward, the absolute plate motions at both sides of the ridge do not move apart symmetrically, but in similar directions and at increasingly different speeds.

In Figures 2e and 3e, most of the plume is located below the African plate, but the plate motions still push it toward the ridge, thereby increasing the tilt of the plume tail. Consequently, melting still occurs at the ridge, not beneath the African plate. This differs significantly from other hotspots such as Tristan, where the plume jumps completely to the other plate due to plate motions directed away from both sides of the Mid-Atlantic Ridge [*Gassmöller et al*., 2016].

In the subsequent evolution of the simulation, the plume moves further underneath the African plate, while plume and ridge are still interacting (Figures 2f and 3f). At 10 Ma, the upper part of the plume shape becomes more spherical and off-ridge-like, but it is still connected to the ridge (Figures 2g and 3g). From the west, Madagascar and the eastern tip of Africa move into the model domain (Figures 3e–3h), agreeing with the extent of the model box in Figure 1. Figures 2h and 3h represent the present-day state of the plume. The tail is extremely tilted—stronger than in the global model, which was used to determine the plume inflow position in the model box—and stretched toward the ridge and while the shape resembles an off-ridge state, melting does not occur at the position of the plume arrival approximately below La Réunion Island, but only much closer toward the ridge below thinner lithosphere.

3.2. Predicted Crustal Thickness Map

The crustal thickness map (Figure 4) is computed as described in section 2.1 and shows the present-day pattern of the Réunion hotspot track as predicted by the numerical model. For reasons of clarity, the figure shows only the crust produced by the plume and neglects the crust that is generated separately at the mid-ocean ridges. This is achieved by subtracting the result of the same model without a plume from the result of the original model, thus leaving the contribution of the plume.

Assuming that topography and crustal thickness correspond to each other, the general resemblance with the currently observable hotspot track is evident (dark red outlines in Figure 4 or topography in Figure 1). Accurate comparisons can also be achieved with crustal thickness estimates from previous studies in this region, either determined by gravity anomaly inversion (such as shown in Figure 1 in *Torsvik et al*. [2013], which reaches maximum crustal thickness values of about 35 km in several areas of the hotspot track), based on seismic refraction profiles (such as *Charvis et al*. [1999] and *Gallart et al*. [1999]) or obtained from receiver function studies (such as *Gupta et al*. [2010] or *Fontaine et al*. [2015]). Apart from single peak values, the maximum crustal thickness of Figure 4a is about 45 km. More detailed comparisons for individual islands are described in section 4.2.

While many features of the observed hotspot track are matched well by the model, one prominent disagreement is the position of the Deccan Traps. Although the plume reaches the base of the lithosphere below the observed location of the LIP, the continental lithosphere of India is too thick to enable melting in the model. Possible explanations for this disagreement are discussed in section 4.1.

The Laccadives and Maldives, however, appear as island chains at their correct positions (although the northern end of the Laccadives seems to be misplaced along with the Deccan Traps). Moreover, a narrow gap in the track is visible around 2°S between the Maldives and Chagos. This result remarkably coincides with the topography and is generated even though the plume inflow in the model is continuous and unchanged over time. The physical processes creating the gap are described in detail in section 3.4.

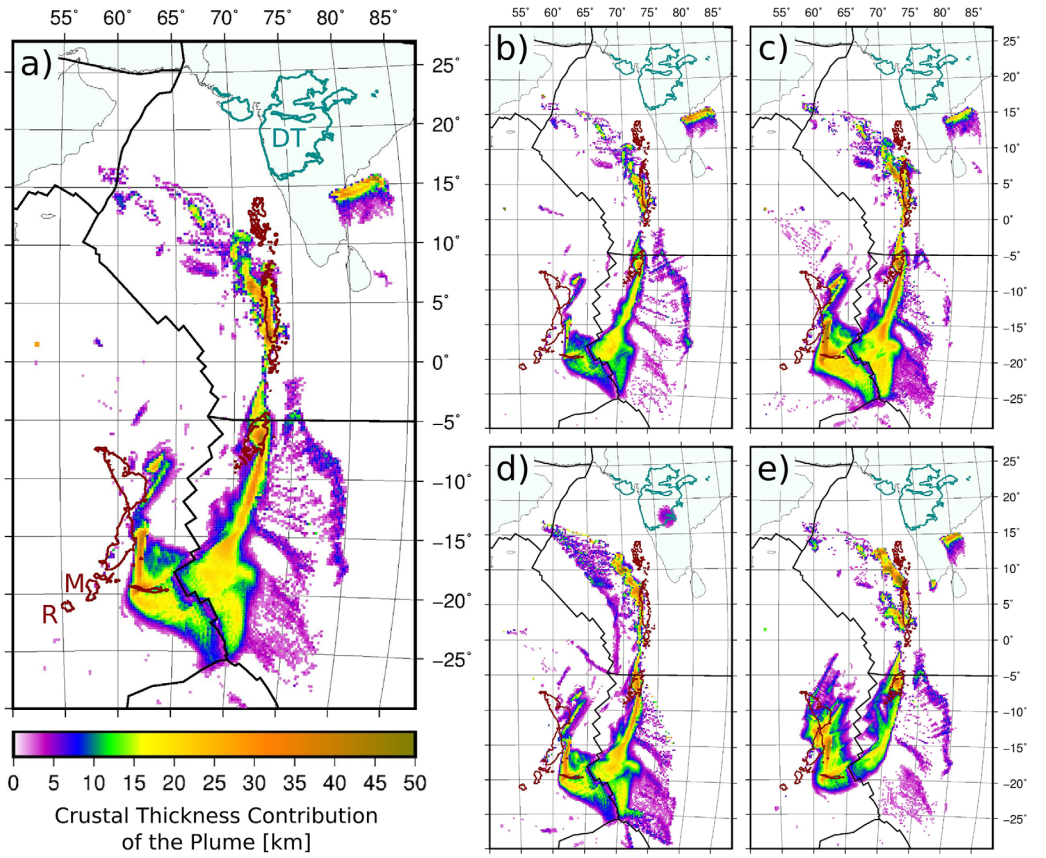

Figure 4. Present-day model state: crustal thickness pattern solely produced by the plume in various models. (a) Reference Model without any crust at the Deccan Traps (DT) or close to Mauritius (M) or Réunion (R). (b) DeltaT200, (c) DeltaT300, (d) HomLith, and (e) NoGlobalFlow. The dark red outlines show the observed hotspot track, represented by the −1500 m topography contours.

The shape of the predicted Chagos Bank resembles the topographic appearance as well. Further south on the Australian plate, the model predicts a wide area covered by crust that is not observed in the topography. This is caused by the long-term plume-ridge interaction already noted during the model evolution. On the African side, the Mascarene Plateau appears shifted to the East and not as prominent as in the topography. As seen in the model development, no crust at all is generated at Mauritius or La Réunion Island. Consequently, the youngest part of the hotspot track differs from observations, although the plume arrives at the base of the lithosphere close to La Réunion Island, and potential reasons for this are discussed in section 4.1.

An interesting young feature that nevertheless fits the observations is the long crustal segment heading from Mauritius toward the Central Indian Ridge—it is slightly rotated (trending from east-northeast to west-southwest compared to the east-west running topographic feature), but clearly resembles the shape of the Rodrigues Ridge. A thorough explanation for the origin of this feature can be found in section 3.5.

3.3. Effects of Parameter Variations

Figures 4b–4e show a selection of crustal thickness maps achieved by varying one parameter in contrast to the reference model in each case. Additional maps can be found in supporting information Figure S3. In particular, the properties of the plume were varied to investigate which model generates a realistic crustal thickness, and the plume inflow position over time was varied to illuminate which hotspot motion model matches the observed distribution of magmatic crust best. To ensure that the inflow velocity of the plume at the bottom of the model domain stays consistent with the velocity of the plume inside the model for different model setups, the plume excess temperature ΔT_{tail}, the inflow velocity v_{tail}, and the inflow area $A_{tail} = \pi R_{tail}^2$ are changed collectively, such that $\Delta T_{tail}\, A_{tail}\, v_{tail}^{-1} = \text{const.}$ in agreement with Stokes' law for the rising

or sinking velocity of a sphere in a viscous medium. The main results of the parameter variations are as follows:

1. Decreasing the excess temperature of the plume tail to 200 K (model DeltaT200, Figure 4b) results in a smaller amount of crust distributed over a smaller area and reduces the maximum crustal thickness to about 40 km. Increasing the excess temperature to 300 K (model DeltaT300, Figure 4c) has the opposite effect and yields about 50 km of maximum crustal thickness.
2. Varying the plume's buoyancy flux (models Flux950 and Flux1900) has very similar effects: the amount of crust, the thickness, and width of the hotspot track decrease with decreasing buoyancy flux, while an increase has the contrary effect.
3. Keeping the plume inflow position constant at its initial position underneath the Deccan Traps (model FixedPlume) alters the recent part of the hotspot track such that it fits the topographic map slightly better than the result of the reference model.
4. Even for a plume motion starting 140 km further north and ending 400 km west of the respective positions of the reference model (model PlumePosVar5), the Deccan Traps are still misplaced on thin oceanic lithosphere. Also the tilt of the plume tail gets even stronger and present-day melting still takes place at the Central Indian Ridge, not closer to La Réunion.
5. In model PlumePosVar9, the plume inflow starts at the same position as in the reference model, but moves westward in order to position the present-day plume underneath La Réunion Island at the boundary between lithosphere and asthenosphere. However, melting is still not initiated at La Réunion.
6. Model LithThickNew uses input files based on the LITHO1.0 model of *Pasyanos et al*. [2014] with the intention of using a different lithosphere thickness distribution underneath India that might lead to correctly located Deccan Traps, but the result shows only minor differences from the reference model.
7. Switching to the simplified assumption of a homogeneous lithosphere thickness with a half-space cooling age of 55 Myr (model HomLith, Figure 4d) enables melting at the site of the Deccan Traps, because the uniformly 125 km thick lithosphere is much thinner than the continental lithosphere in the reference model.
8. *Gassmöller et al*. [2016] reported the strong impact of the global flow on the tilt of the plume tail and the associated change of the melt volume. Despite the changes in rheology, this observation seems to be equally valid in the case of the Réunion model (model NoGlobalFlow, Figure 4e). Altogether, the crustal thickness pattern without applied global flow seems to match the topographic pattern better than the result of the reference model, especially in the southern part of the hotspot track and the Mascarene Plateau, because the much less tilted plume tail positions the plume much earlier underneath the African plate (see supporting information Figures S1 and S2).
9. Excluding the rheological effect of dehydration (model NoDehyd) leads to an enormously increased crustal thickness exceeding 100 km.
10. Neglecting the effect of the depletion buoyancy (model NoDepl) hardly differs from the result of the reference model.
11. In model DefaultVisc, the viscosity inside the plume is higher and the viscosity contrast between plume and ambient mantle is lower than in the reference model. This leads to a slightly broader and less tilted plume, but does not significantly change the crustal thickness pattern.

In summary, regarding the properties of the plume, model DeltaT200 with a plume temperature of 200 K and a buoyancy flux of ~800 kg/s produces a maximum crustal thickness of about 40 km that agrees best with the maximum of about 35 km reported by *Torsvik et al*. [2013]. Concerning the plume inflow position over time, model PlumePosVar9 features a plume that arrives below the reconstructed position of the Deccan Traps, reproduces the observed topography of the hotspot track and reaches the base of the lithosphere below La Réunion Island at present day. While this means that the plume motion model seems to agree well with observations, there is still no melt generated at the position of the Deccan Traps and La Réunion, which is discussed in more detail in section 4.1.

The most important finding, however, is that the gap between the Maldives and Chagos as well as the Rodrigues Ridge are clearly reproduced more or less distinct in all the varied model setups despite the parameter modifications. The origins of these features are therefore described in more detail in the following two sections.

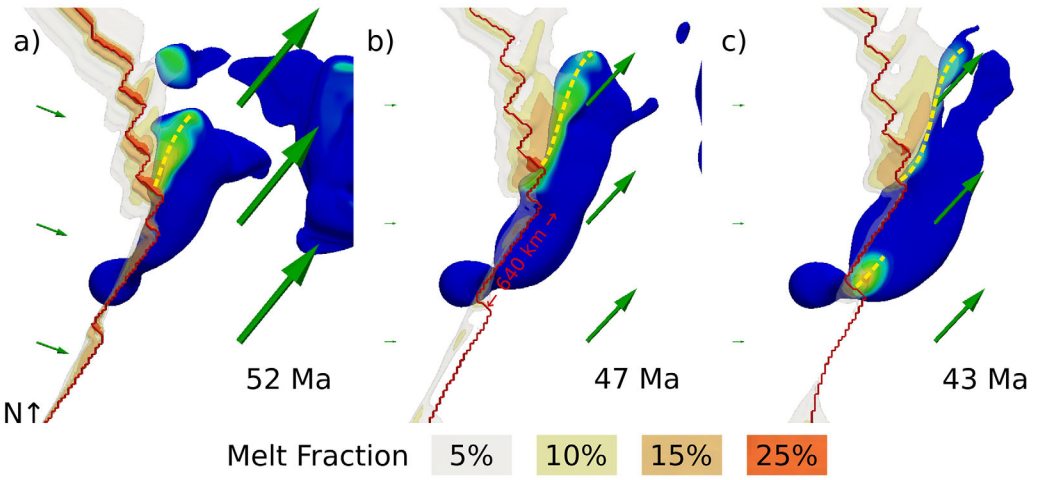

Figure 5. Top view of the plume (colored as in Figure 2) illustrating the formation of the gap in the hotspot track. Green arrows depict the velocities of the African and Indian plate and the isosurfaces along the Central Indian Ridge (red line) show total melt fractions above 5% in the entire model domain. The dashed yellow lines represent the zones where the Laccadives and Maldives are created, followed by the Chagos archipelago after the gap.

3.4. Formation of the Gap in the Hotspot Track

The gap interrupting the typically continuous hotspot track between the Maldives and the Chagos Bank was formed around 50 Ma, approximately coinciding with the India-Asia collision [*Patriat and Achache*, 1984]. In the numerical model, this tectonic event is indirectly considered by the abrupt velocity decrease of the Indian plate at 50 Ma (note the velocity difference between Figures 2b and 2c or Figures 5a and 5b, respectively). However, since the direction of the Indian plate motion hardly changes, this has only a minor effect on the creation of the gap, which is illustrated in Figure 5 (see supporting information Movie S1 for an animated view).

The ridge geometry (illustrated by the red line) appears as a series of steps, reflecting the distribution of transform faults at the Central Indian Ridge. While decompression melting occurs along the ridge axis, almost no melt is generated along the transform faults. At 52 Ma (Figure 5a), the hot rising plume material is in the vicinity of the ridge axis, coinciding with the place of origin of the Laccadives and Maldives (dashed yellow line). Over time, the ridge moves northeastward and the plume surface position migrates accordingly southward along the ridge, jumping from one ridge segment to another and as long as the transform faults are sufficiently small, this process results in continuous island chains on the Indian plate. But at 47 Ma (Figure 5b), the plume is located underneath a particularly long transform fault that disrupts the melt generation and thus creates a gap until the plume reaches the next ridge segment around 44 Ma. At this time melting starts again and the Chagos archipelago is formed (second dashed yellow line in Figure 5c). While the position of the gap fits observations very well, the timing is slightly shifted: age estimations at the northern end of the Chagos Bank yielded 49.3 Myr $\pm$ 0.6 Myr [*Duncan and Hargraves*, 1990] instead of 44 Myr observed in the model, a difference that could be easily explained by a slightly shifted plume position.

In conclusion, the gap in the model originates from a combination of the ridge geometry, in particular the distribution of transform faults, plate motions and plume-ridge interaction. This result differs significantly from previous studies that investigated similar phenomena and explained the gaps between off-ridge and on-ridge hotspot tracks by plume material being ponded by membrane compression [*Sleep*, 2002] or attributed the formation of discrete islands within a hotspot track to shear instabilities of the involved mantle plume [*Skilbeck and Whitehead*, 1978; *Ihinger*, 1995], solitary waves in the plume [*Schubert et al.*, 1989] or the interaction of rising magma and lithospheric flexure [*Hieronymus and Bercovici*, 1999].

3.5. Origin of the Rodrigues Ridge

The Rodrigues Ridge is a narrow volcanic lineament that was formed between 10 and 7 Ma [*Dyment et al.*, 2007] and seems to connect the younger end of the Réunion hotspot track with the closest part of the Central Indian Ridge, which is located more than 1000 km east of Réunion Island. The pronounced west-east

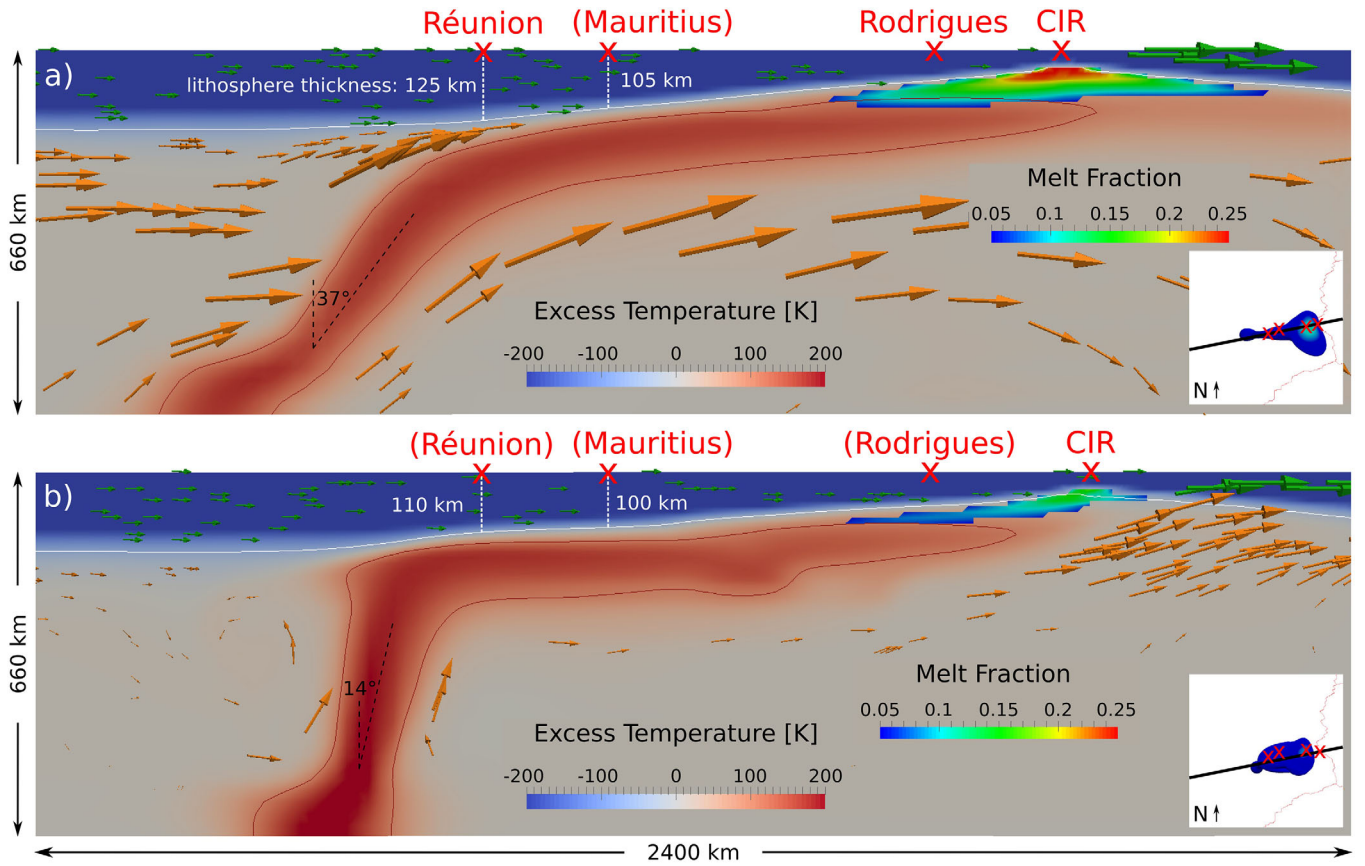

Figure 6. Cross sections of the present-day state showing the sublithospheric flow channel from the Réunion plume along the Rodrigues Ridge toward the Central Indian Ridge (CIR) in (a) model PlumePosVar9 and (b) model NoGlobalFlow, slightly shifted to the south to cut through the plume conduit. Colors show the excess temperature relative to the adiabat and the area exceeding 5% melt fraction, respectively. The dark red contour outlines the plume and the white contour the base of the lithosphere. Orange arrows depict the global flow, green arrows the plate motions. The inset map shows the position of the cross section in a top view of the model.

trend of the Rodrigues Ridge deviates from the northeastward motion of the African plate and the regular hotspot track along the Mascarene Plateau. Despite the great distance, the Rodrigues Ridge seems to be evidence of plume-ridge interaction as indicated by the geochemical anomaly around 20°S at the Central Indian Ridge [*Mahoney et al.*, 1989; *Schilling*, 1991; *Nauret et al.*, 2006; *Füri et al.*, 2011]. The first qualitative interpretation of this unusual feature was given by *Morgan* [1978], who explained the long-distance plume-ridge interaction by an asthenospheric channel in which plume material is flowing toward the ridge.

All crustal thickness maps predicted by the model variations (Figure 4 and supporting information Figure S3) show a distinctive, although slightly rotated crustal lineament at the position of the Rodrigues Ridge. Supporting information Movie S1 reveals that its origin is strongly dependent on the ridge geometry, similar to the formation of the gap between the Maldives and the Chagos Bank in the hotspot track (see section 3.4). A major feature in ridge geometry in this region is the Marie Celeste Fracture Zone (Figure 1), a transform fault where no decompression melting occurs over the last 20 Myr in the model. During this time, the plume material approaches the surface southwest of the fracture zone and then flows toward the closest part of the ridge, in this case the corner between the Marie Celeste Fracture Zone and the adjacent ridge segment. Hence, over an extended period of time, melt is always produced at the southwestern end of the fracture zone, and the generated crust forms a lineament parallel to it. It appears like a prolongation of the Marie Celeste Fracture Zone and thus resembles a slightly rotated Rodrigues Ridge.

Figure 6a shows the present-day state of the plume in a cross section of model PlumePosVar9, where the plume reaches the lithosphere-asthenosphere boundary underneath La Réunion (see white dashed line). The combined effects of the plate motions, the global flow, upside-down drainage, and negative dynamic pressures generated by the plate motions at the ridge direct the uprising plume material toward regions of

thinner lithosphere at the Central Indian Ridge. In spite of the long distance, the plume reaches the ridge axis where the lithosphere is thin enough to initiate melting in an area extending as far as the Rodrigues Ridge. This explicitly supports the existing hypothesis of continuous long-distance plume-ridge interaction and the existence of a sublithospheric flow channel [*Morgan*, 1978]. The same also applies for the almost vertical plume in model NoGlobalFlow (Figure 6b), where the plume material still flows toward the ridge and melting occurs almost exclusively underneath the African plate.

4. Discussion

4.1. Melt Generation at the Deccan Traps and Réunion Island

The main focus of this study is the interaction of the Réunion plume with the Central Indian Ridge, and the presented models plausibly explain the development of the gap in the hotspot track between the Maldives and the Chagos Bank and the creation of the Rodrigues Ridge. However, crustal production below the lithosphere further away from the ridge is not captured as well. In particular, both the beginning and the end of the modeled hotspot track deviate from observations: no melt is generated on the Indian continent—at the reconstructed position of the Deccan Traps—and the present-day plume does not produce any melt close to La Réunion or Mauritius. In both cases, the plume in model PlumePosVar9 reaches the base of the lithosphere at the position expected from observations (below India and Réunion Island, respectively), but does not melt because of the high lithospheric thickness (>200 km for India, 125 km for La Réunion, and 105 km for Mauritius; see Figure 6a). Instead, hot plume material flows toward regions of thinner lithosphere, where melt is generated due to decompression.

There are a number of potential explanations for this behavior. First, the models potentially overestimate the lithospheric thickness, and employing a model that predicts thinner lithosphere could lead to a more realistic melt production away from the ridge (as demonstrated by the correctly located Deccan Traps in model HomLith, Figure 4d). In the case of India, the continental lithosphere might have been thinner before the plume impingement, and some of the thick lithosphere visible in seismic models today may have been generated during and after the massive melting event of the plume through dehydration stiffening. For Mauritius and La Réunion, lithospheric thickness is not generated self-consistently in the model, because it was created outside the model domain. Instead, the thermal structure is prescribed as a boundary condition based on lithospheric age models (see section 2.2). Plate-cooling models such as GDH1 [*Stein and Stein*, 1992] predict thinner lithosphere for a given lithospheric age than the half-space cooling model utilized in this study and could therefore possibly facilitate melting at La Réunion Island. Much thinner lithosphere has also been suggested by a recent receiver function study [*Fontaine et al*., 2015], which estimated 70 km thick lithosphere beneath La Réunion and 50 km thick lithosphere underneath Mauritius—values small enough to enable melting underneath these islands and thus yield a more realistic present-day crustal distribution as a model result.

Second, the modeled plume does neither contain enriched components like eclogite, which would lead to melting at higher pressures [*Sobolev et al*., 2007, 2011], nor volatiles, known to decrease the solidus of mantle rocks [e.g., *Katz et al*., 2003]. For the case of La Réunion, a plume with an excess temperature of 200 K containing recycled crust would already start to melt at 180 km depth [*Sobolev et al*., 2011], whereas the modeled purely thermal (peridotitic) plume only starts to melt at 115 km depth, closer to the ridge (see Figure 6). In the case of the Deccan Traps, as soon as melting occurs, the amount of melt could be tremendously increased by thermomagmatic erosion of the lithosphere [*Sobolev et al*., 2011], a mechanism that is related to the transport and reaction of generated melt, and is not included in the models. Other disregarded processes such as dislocation creep could also lead to mechanical thinning of the lithosphere above the plume, thus increasing melt production.

By optimizing the lithospheric thickness used as initial and boundary conditions and the composition of the plume, the geodynamic model could presumably be tuned to also reproduce the magmatic crust generated at Réunion Island and the Deccan Traps. However, as the focus is on plume-ridge interaction, this is outside the scope of the present study.

It has recently been proposed by *Glišović and Forte* [2017]—who reconstruct large-scale plume and mantle structures in the past based on present-day seismic tomography in contrast to the forward modeling approach and much higher resolved plume in this study (due to a considerably smaller model domain and

the adaptive mesh refinement)—that the northern part of the Deccan Traps was generated by an additional unrecognized plume underneath the Comoros. Since this study is not designed to handle melting in continental environments, a second plume beneath India around 65 Ma would likely result in additional flow toward thinner oceanic lithosphere (regardless of a correct plume timing and position as discussed above). However, the model evolution does not indicate a need for a second plume to accurately shape the Réunion hotspot track.

4.2. Crustal Thickness Values

The overall crustal thickness contribution of the plume predicted by the models is approximately in the same range as what is inferred from observations, in particular in comparison to models of plume-ridge interaction without dehydration rheology where the crust generated by the plume exceeds 100 km (supporting information Figure S3g or models in *Gassmöller et al*. [2016]). A plume with an excess temperature of 200 K (model DeltaT200) produces up to 40 km of magmatic crust (see Figure 4b), which is comparable to the crustal thickness map of *Torsvik et al*. [2013] that features maximum values of about 35 km at the Maldives, the Chagos Bank, and the Mascarene Plateau.

Nevertheless, the model predictions still exceed the expected values, especially when taking into account that the crust produced at the mid-ocean ridges (which is not included in Figure 4) contributes additionally to the absolute values, and that *Torsvik et al*. [2013] attribute the thick crust partly to underlying continental fragments.

More detailed comparisons of model DeltaT200 with results from previous studies in the region of the hotspot track also indicate that the model results are at the upper end of the range of expected values. For the Laccadives, the inversion of teleseismic receiver functions of *Gupta et al*. [2010] reported an oceanic crust of 16 km thickness underplated by an 8 km thick high-velocity layer, while the modeled plume produces about 25 km excess crustal thickness. For the Maldives, the receiver function study of *Fontaine et al*. [2015] estimated 6–7 km crust and a 14–11 km thick underplated layer, whereas the modeled plume generates up to 40 km excess crustal thickness. From bathymetry and gravity data, *Henstock and Thompson* [2004] modeled mean crustal thicknesses of 12–27 km for the Chagos-Laccadive ridge. *Fontaine et al*. [2015] suggested 8 km crust and a 5 km thick underplated layer underneath Chagos; the plume in the model produces excess crustal thickness of up to 35 km. On the African plate, *Fontaine et al*. [2015] identified 10 km crust and a 7 km thick underplated layer underneath Mauritius, 6 km crust and a 2 km thick underplated layer underneath La Réunion and 6 km crust beneath Rodrigues. Along the Rodrigues Ridge, the modeled plume yields up to 30 km excess crustal thickness. In summary, the published estimates indicate that the excess temperature of the plume is most likely at the lower end of values tested in this study (i.e., model DeltaT200).

A potential explanation for the higher values in the computation is the fact that the used melting model [*Katz et al*., 2003] is an equilibrium batch melting model (as opposed to a fractional melting model). While it considers the decrease in melt productivity with increasing depletion, this effect would be even stronger in case of fractional melting, due to the associated changes in composition. As incremental batch melting—presumably occurring in a mantle plume—has a productivity somewhere between batch melting and fractional melting, the models overestimate the amount of generated crust.

Moreover, the melt extraction method applied in this study considers the entirety of plume induced melt to ascend through the lithosphere and create crustal material—whereas melt close to a mid-ocean ridge is expected to migrate toward the ridge instead of rising vertically [*Braun and Sohn*, 2003]. The neglect of possible lateral melt transport could therefore also provide an explanation for the high amounts of crust produced by the modeled plume.

4.3. Global Flow and Present-Day State of the Plume

At the present-day state of the model, the plume is highly tilted (by approximately 37°) and most of the plume material is drawn eastward, in the direction of the Central Indian Ridge. If the plume inflow position is manually moved further away from the ridge as in model PlumePosVar5, the tilt is even more pronounced (approximately 39°). Comparing the reference model or model PlumePosVar9 with the tilt of 14° in model NoGlobalFlow (Figures 6a and 6b, respectively, or supporting information Movie S1) provides evidence that the main factor which deflects the plume from its vertical ascent is the global flow prescribed as boundary conditions.

In the global mantle convection model from which the boundary input files are derived, the global flow at the latitude of the Réunion plume at recent times is vastly influenced by the fast ascent of hot material above the African LLSVP. The main direction of the global flow is therefore eastward, relatively fast and almost unaffected by the (relatively slow) northeastward plate motions above. This provides an explanation why the plume in the reference model is deflected more to the east than to the northeast and consequently produces melt too far south along the Central Indian Ridge, whereas the plume-ridge interaction in model NoGlobalFlow matches the region of the plume-related geochemical anomaly between 12°S and 22°S along the ridge [*Schilling*, 1991] (Figures 4a and 4e, respectively). The direction of the modeled plume tilt is consistent with the plume tilt in the global model from which the global flow is derived—between east-northeastward and northeastward at present.

One possible explanation for this major role of the global flow in the model, and that it deflects plume material to a part of the ridge where no geochemical anomaly or excess crustal thickness is observed, could be that large-scale mantle circulation is in fact more sluggish than prescribed in the model, a view recently championed by Kevin Burke [*Torsvik et al*., 2016]. Considering that the much more vertical plume tail in model NoGlobalFlow produces a crustal thickness pattern that fits the topography of the southern part of the hotspot track well—especially the Mascarene Plateau and the region along the Central Indian Ridge up to the Rodrigues Triple Junction (Figure 4e)—an optimized model of global mantle flow would likely feature slower movements and a flow direction slightly rotated to the northeast in accordance with the plate motions.

To compare the geodynamic model results to seismological tomographic models or shear-wave splitting observations, the present-day state of the model is essential. Figure 6 shows two feasible model predictions for the current state of the plume, reaching the base of the lithosphere under Réunion Island (even though no melt is generated there, as discussed above). Consistent with the northeastward large-scale plate motion and the eastward global flow—and the idea of an Indian Ocean "conveyor belt" [*Becker and Faccenna*, 2011]—the plume approaches La Réunion from west-southwest, the direction of the LLSVP at the core-mantle boundary. In contrast to a recent seismic anisotropy analysis beneath islands on or close to the hotspot track, which suggested the plume conduit to be located 100–200 km north of La Réunion Island [*Barruol and Fontaine*, 2013], the plume in the models presented in this study arrives below the lithosphere close to La Réunion as in previous models [*Steinberger*, 2000; *Steinberger and Antretter*, 2006; *Boschi et al*., 2007; *Steinberger and Torsvik*, 2012] and consistent with global seismological studies by *Montelli et al*. [2006] and model SMEAN2 (see supporting information Figure S4 for a cross section of the Réunion plume). More insights on the present-day state and particularly the tilt of the plume are to be expected from the seismological results of the RHUM-RUM project.

5. Conclusions and Outlook

The motive for this study was to investigate the interaction between the Réunion plume and the Central Indian Ridge, and how it shaped the crustal thickness pattern of the Réunion hotspot track. Comparing the model results to the observed topographic expression of the hotspot track, the following conclusions can be drawn:

The continuous ocean-island chains of the Laccadives and Maldives fit into the widely accepted concept of an age-progressive hotspot track. The subsequent gap in the hotspot track between the Maldives and the Chagos Bank does not contradict this interpretation. Rather it is a direct consequence of the interaction between the Central Indian Ridge and the Réunion plume, which at this time moved along a particularly long ridge transform fault, thus creating a pause in volcanic activity. Only after the ridge traveled far enough for the plume to arrive close to the next ridge segment, the Chagos Bank was generated. This conclusion holds true for all variations of model parameters in this study.

After the Central Indian Ridge overrode the plume, the edge between the Marie Celeste Fracture Zone and the adjacent ridge segment acted as a focal point to which a part of the plume material was dragged and where thinner lithosphere enabled melting and the creation of the Rodrigues Ridge. This provides computational support for the theory of *Morgan* [1978], showing that plume-ridge interaction is possible up to distances on the order of 1000 km. Altogether, the models illustrate how small-scale surface features originate from the complex interaction between processes in the mantle and the lithosphere.

As discussed above, to capture the full plume evolution from the Large Igneous Province to the melt generation beneath La Réunion today, a number of additional complexities will need to be considered. In particular, a more complex melt generation model that includes enriched source components in the plume, and the potential for thermomagmatic erosion is required to accurately model the generation of a Large Igneous Province on thick continental lithosphere. Additionally, to resolve the generation of volcanic chains as narrow features (like the Rodrigues Ridge) as opposed to broad zones of magmatic crust, a plastic material rheology coupled to a melt migration model might proof crucial to achieve the necessary focusing of melt.

At the present-day state, the modeled plume arrives approximately below La Réunion Island and features a strong eastward tilt in the upper mantle, even though the plates are moving northeastward. The models suggest that this tilt is mainly caused by the eastward surrounding flow field. Although the speed of global mantle flow is debated (as discussed above), comparisons between the model results, in particular the degree of plume tilting, and future high-resolution seismic studies within the RHUM-RUM project will therefore allow to estimate the actual speed of upper mantle flow below the Indian Ocean.

Acknowledgments
The geodynamic models were computed with the open-source software ASPECT (http://aspect.dealii.org) and the necessary data to reproduce the models is included in the supporting information. The constructive comments of two anonymous reviewers have been appreciated. This project is funded by the Deutsche Forschungsgemeinschaft (DFG) under grant STE 907/11–1 to B.S. as part of the RHUM-RUM project (Réunion Hotspot and Upper Mantle—Réunions Unterer Mantel). The computational resources were provided by the North-German Supercomputing Alliance (HLRN) as part of project bbp00006: "Numerical geodynamic modeling of a mantle plume under La Réunion and its interaction with large-scale 3-D mantle flow." J. D. and R. G. were partially supported by the Computational Infrastructure for Geodynamics initiative (CIG), through the National Science Foundation under Awards EAR-0949446 and EAR-1550901, administered by The University of California-Davis, and the National Science Foundation under award OCI-1148116 as part of the Software Infrastructure for Sustained Innovation (SI2) program.

References

Ashwal, L. D., M. Wiedenbeck, and T. H. Torsvik (2017), Archaean zircons in Miocene oceanic hotspot rocks establish ancient continental crust beneath Mauritius, *Nat. Commun.*, *8*, 14,086, doi:10.1038/ncomms14086.

Bangerth, W., J. Dannberg, R. Gassmöller, T. Heister, et al. (2017), *ASPECT: Advanced Solver for Problems in Earth's ConvecTion*, Comput. Infrastruct. for Geodyn., Davis, Calif.

Barruol, G., and F. R. Fontaine (2013), Mantle flow beneath la Réunion hotspot track from SKS splitting, *Earth Planet. Sci. Lett.*, *362*, 108–121, doi:10.1016/j.epsl.2012.11.017.

Barruol, G., and K. Sigloch (2013), Investigating La Réunion hot spot from crust to core, *Eos Trans. AGU*, *94*(23), 205–207, doi:10.1002/2013EO230002.

Becker, T. W., and C. Faccenna (2011), Mantle conveyor beneath the Tethyan collisional belt, *Earth Planet. Sci. Lett.*, *310*(3–4), 453–461, doi:10.1016/j.epsl.2011.08.021.

Boschi, L., T. W. Becker, and B. Steinberger (2007), Mantle plumes: Dynamic models and seismic images, *Geochem. Geophys. Geosyst.*, *8*, Q10006, doi:10.1029/2007GC001733.

Braun, M. G., and R. A. Sohn (2003), Melt migration in plume-ridge systems, *Earth Planet. Sci. Lett.*, *213*(3–4), 417–430, doi:10.1016/S0012-821X(03)00279-6.

Burke, K., B. Steinberger, T. H. Torsvik, and M. A. Smethurst (2008), Plume generation zones at the margins of large low shear velocity provinces on the core-mantle boundary, *Earth Planet. Sci. Lett.*, *265*(1–2), 49–60, doi:10.1016/j.epsl.2007.09.042.

Cande, S. C., and D. R. Stegman (2011), Indian and African plate motions driven by the push force of the Reunion plume head, *Nature*, *475*(7354), 47–52, doi:10.1038/nature10174.

Charvis, P., A. Laesanpura, J. Gallart, A. Hirn, J.-C. Lépine, B. de Voogd, T. A. Minshull, Y. Hello, and B. Pontoise (1999), Spatial distribution of hotspot material added to the lithosphere under la Réunion, from wide-angle seismic data, *J. Geophys. Res.*, *104*(B2), 2875–2893, doi:10.1029/98JB02841.

Christensen, U. (1983), Convection in a variable-viscosity fluid: Newtonian versus power-law rheology, *Earth Planet. Sci. Lett.*, *64*(1), 153–162, doi:10.1016/0012-821X(83)90060-2.

Courtillot, V. E., and P. R. Renne (2003), On the ages of flood basalt events, *C. R. Geosci.*, *335*(1), 113–140, doi:10.1016/S1631-0713(03)00006-3.

Courtillot, V., J. Besse, D. Vandamme, R. Montigny, J.-J. Jaeger, and H. Cappetta (1986), Deccan flood basalts at the Cretaceous/Tertiary boundary?, *Earth Planet. Sci. Lett.*, *80*(3), 361–374, doi:10.1016/0012-821X(86)90118-4.

Courtillot, V., G. Féraud, H. Maluski, D. Vandamme, M. G. Moreau, and J. Besse (1988), Deccan flood basalts and the Cretaceous/Tertiary boundary, *Nature*, *333*(6176), 843–846, doi:10.1038/333843a0.

Courtillot, V., A. Davaille, J. Besse, and J. Stock (2003), Three distinct types of hotspots in the Earth's mantle, *Earth Planet. Sci. Lett.*, *205*(3–4), 295–308, doi:10.1016/S0012-821X(02)01048-8.

Crough, S. T. (1983), Hotspot swells, *Ann. Rev. Earth Planet. Sci.*, *11*, 165–193, doi:10.1146/annurev.ea.11.050183.001121.

Davies, G. F. (1988), Ocean bathymetry and mantle convection: 1. Large-scale flow and hotspots, *J. Geophys. Res.*, *93*(B9), 10,467–10,480, doi:10.1029/JB093iB09p10467.

Doubrovine, P. V., B. Steinberger, and T. H. Torsvik (2012), Absolute plate motions in a reference frame defined by moving hot spots in the Pacific, Atlantic, and Indian oceans, *J. Geophys. Res.*, *117*, B09101, doi:10.1029/2011JB009072.

Duncan, R. (1990), The volcanic record of the Réunion hotspot, *Proc. Ocean Drill. Program Sci. Results*, *115*, 3–10, doi:10.2973/odp.proc.sr.115.206.1990.

Duncan, R., and R. Hargraves (1990), $^{40}Ar/^{39}Ar$ geochronology of basement rocks from the Mascarene Plateau, the Chagos Bank, and the Maldives Ridge, *Proc. Ocean Drill. Program Sci. Results*, *115*, 43–51, doi:10.2973/odp.proc.sr.115.141.1990.

Duncan, R. A., and M. A. Richards (1991), Hotspots, mantle plumes, flood basalts, and true polar wander, *Rev. Geophys.*, *29*(1), 31–50, doi:10.1029/90RG02372.

Dupeyrat, L., C. Sotin, and E. M. Parmentier (1995), Thermal and chemical convection in planetary mantles, *J. Geophys. Res.*, *100*(B1), 497–520, doi:10.1029/94JB01189.

Dyment, J., J. Lin, and E. Baker (2007), Ridge-hotspot interactions: What mid-ocean ridges tell us about deep Earth processes, *Oceanography*, *20*, 102–115, doi:10.5670/oceanog.2007.84.

Farley, K., and E. Neroda (1998), Noble gases in the Earth's mantle, *Annu. Rev. Earth Planet. Sci.*, *26*, 189–218, doi:10.1146/annurev.earth.26.1.189.

Fontaine, F. R., G. Barruol, H. Tkalčić, I. Wölbern, G. Rümpker, T. Bodin, and M. Haugmard (2015), Crustal and uppermost mantle structure variation beneath la Réunion hotspot track, *Geophys. J. Int.*, *203*(1), 107–126, doi:10.1093/gji/ggv279.

French, S. W., and B. Romanowicz (2015), Broad plumes rooted at the base of the Earth's mantle beneath major hotspots, *Nature*, *525*(7567), 95–99, doi:10.1038/nature14876.

Füri, E., D. R. Hilton, B. J. Murton, C. Hémond, J. Dyment, and J. M. D. Day (2011), Helium isotope variations between Réunion island and the Central Indian Ridge (17°–21°S): New evidence for ridge-hot spot interaction, *J. Geophys. Res.*, *116*, B02207, doi:10.1029/2010JB007609.
Gallart, J., L. Driad, P. Charvis, M. Sapin, A. Hirn, J. Diaz, B. de Voogd, and M. Sachpazi (1999), Perturbation to the lithosphere along the hot-spot track of la Réunion from an offshore-onshore seismic transect, *J. Geophys. Res.*, *104*(B2), 2895–2908, doi:10.1029/98JB02840.
Garnero, E. J., T. Lay, and A. McNamara (2007), Implications of lower-mantle structural heterogeneity for the existence and nature of whole-mantle plumes, *Spec. Pap. Geol. Soc. Am.*, *430*, 79–101, doi:10.1130/2007.2430(05).
Gassmöller, R., J. Dannberg, E. Bredow, B. Steinberger, and T. H. Torsvik (2016), Major influence of plume-ridge interaction, lithosphere thickness variations, and global mantle flow on hotspot volcanism—The example of Tristan, *Geochem. Geophys. Geosyst.*, *17*, 1454–1479, doi:10.1002/2015GC006177.
Glišović, P., and A. M. Forte (2017), On the deep-mantle origin of the Deccan Traps, *Science*, *355*(6325), 613–616, doi:10.1126/science.aah4390.
Gupta, S., S. Mishra, and S. S. Rai (2010), Magmatic underplating of crust beneath the Laccadive Island, NW Indian Ocean, *Geophys. J. Int.*, *183*(2), 536–542, doi:10.1111/j.1365-246X.2010.04759.x.
Henstock, T. J., and P. J. Thompson (2004), Self-consistent modeling of crustal thickness at Chagos-Laccadive ridge from bathymetry and gravity data, *Earth Planet. Sci. Lett.*, *224*(3–4), 325–336, doi:10.1016/j.epsl.2004.05.021.
Herzberg, C., and E. Gazel (2009), Petrological evidence for secular cooling in mantle plumes, *Nature*, *458*, 619–622, doi:10.1038/nature07857.
Hieronymus, C. F., and D. Bercovici (1999), Discrete alternating hotspot islands formed by interaction of magma transport and lithospheric flexure, *Nature*, *397*(6720), 604–607, doi:10.1038/17584.
Hirth, G., and D. Kohlstedt (2003), Rheology of the upper mantle and the mantle wedge: A view from the experimentalists, in *Inside the Subduction Factory*, edited by J. Eiler, pp. 83–105, AGU, Washington, D. C., doi:10.1029/138GM06.
Hofmann, C., G. Féraud, and V. Courtillot (2000), $^{40}Ar/^{39}Ar$ dating of mineral separates and whole rocks from the Western Ghats lava pile: Further constraints on duration and age of the Deccan traps, *Earth Planet. Sci. Lett.*, *180*(1–2), 13–27, doi:10.1016/S0012-821X(00)00159-X.
Howell, S. M., G. Ito, A. J. Breivik, A. Rai, R. Mjelde, B. Hanan, K. Sayit, and P. Vogt (2014), The origin of the asymmetry in the Iceland hotspot along the Mid-Atlantic Ridge from continental breakup to present-day, *Earth Planet. Sci. Lett.*, *392*, 143–153, doi:10.1016/j.epsl.2014.02.020.
Ihinger, P. D. (1995), Mantle flow beneath the Pacific plate: Evidence from seamount segments in the Hawaiian-Emperor chain, *Am. J. Sci.*, *295*, 1035–1057, doi:10.2475/ajs.295.9.1035.
Ito, G., Y. Shen, G. Hirth, and C. J. Wolfe (1999), Mantle flow, melting, and dehydration of the Iceland mantle plume, *Earth Planet. Sci. Lett.*, *165*(1), 81–96, doi:10.1016/S0012-821X(98)00216-7.
Jay, A. E., and M. Widdowson (2008), Stratigraphy, structure and volcanology of the SE Deccan continental flood basalt province: Implications for eruptive extent and volumes, *J. Geol. Soc.*, *165*(1), 177–188, doi:10.1144/0016-76492006-062.
Katz, R. F., M. Spiegelman, and C. H. Langmuir (2003), A new parameterization of hydrous mantle melting, *Geochem. Geophys. Geosyst.*, *4*(9), 1073, doi:10.1029/2002GC000433.
Kronbichler, M., T. Heister, and W. Bangerth (2012), High accuracy mantle convection simulation through modern numerical methods, *Geophys. J. Int.*, *191*(1), 12–29, doi:10.1111/j.1365-246X.2012.05609.x.
Mahoney, J. J., J. H. Natland, W. M. White, R. Poreda, S. H. Bloomer, R. L. Fisher, and A. N. Baxter (1989), Isotopic and geochemical provinces of the western Indian Ocean spreading centers, *J. Geophys. Res.*, *94*(B4), 4033–4052, doi:10.1029/JB094iB04p04033.
Manglik, A., and U. R. Christensen (1997), Effect of mantle depletion buoyancy on plume flow and melting beneath a stationary plate, *J. Geophys. Res.*, *102*(B3), 5019–5028, doi:10.1029/96JB03623.
McKenzie, D., and J. Sclater (1971), The evolution of the Indian Ocean since the Late Cretaceous, *Geophys. J. Int.*, *24*, 437–528, doi:10.1111/j.1365-246X.1971.tb02190.x.
Montelli, R., G. Nolet, F. A. Dahlen, G. Masters, E. R. Engdahl, and S.-H. Hung (2004), Finite-frequency tomography reveals a variety of plumes in the mantle, *Science*, *303*(5656), 338–343, doi:10.1126/science.1092485.
Montelli, R., G. Nolet, F. A. Dahlen, and G. Masters (2006), A catalogue of deep mantle plumes: New results from finite-frequency tomography, *Geochem. Geophys. Geosyst.*, *7*, Q11007, doi:10.1029/2006GC001248.
Morgan, W. J. (1971), Convection plumes in the lower mantle, *Nature*, *230*, 42–43, doi:10.1038/230042a0.
Morgan, W. J. (1978), Rodriguez, Darwin, Amsterdam,. . ., A second type of Hotspot Island, *J. Geophys. Res.*, *83*(B11), 5355–5360, doi:10.1029/JB083iB11p05355.
Müller, R. D., M. Sdrolias, C. Gaina, and W. R. Roest (2008), Age, spreading rates, and spreading asymmetry of the world's ocean crust, *Geochem. Geophys. Geosyst.*, *9*, Q04006, doi:10.1029/2007GC001743.
Nauret, F., W. Abouchami, S. Galer, A. Hofmann, C. Hémond, C. Chauvel, and J. Dyment (2006), Correlated trace element-Pb isotope enrichments in Indian MORB along 18–20°S, Central Indian Ridge, *Earth Planet. Sci. Lett.*, *245*(1–2), 137–152, doi:10.1016/j.epsl.2006.03.015.
Officer, C. B., A. Hallam, C. L. Drake, and J. D. Devine (1987), Late Cretaceous and paroxysmal Cretaceous/Tertiary extinctions, *Nature*, *326*(6109), 143–149, doi:10.1038/326143a0.
Pasyanos, M. E., T. G. Masters, G. Laske, and Z. Ma (2014), LITHO1.0: An updated crust and lithospheric model of the Earth, *J. Geophys. Res. Solid Earth*, *119*, 2153–2173, doi:10.1002/2013JB010626.
Patriat, P., and J. Achache (1984), India-Eurasia collision chronology has implications for crustal shortening and driving mechanism of plates, *Nature*, *311*(5987), 615–621, doi:10.1038/311615a0.
Putirka, K. (2008), Excess temperatures at ocean islands: Implications for mantle layering and convection, *Geology*, *36*(4), 283–286, doi:10.1130/G24615A.1.
Ribe, N. M., and U. R. Christensen (1999), The dynamical origin of Hawaiian volcanism, *Earth Planet. Sci. Lett.*, *171*(4), 517–531, doi:10.1016/S0012-821X(99)00179-X.
Richards, M. A., R. A. Duncan, and V. E. Courtillot (1989), Flood Basalts and Hot-Spot Tracks: Plume Heads and Tails, *Science*, *246*, 103–107, doi:10.1126/science.246.4926.103.
Schilling, J.-G. (1991), Fluxes and excess temperatures of mantle plumes inferred from their interaction with migrating mid-ocean ridges, *Nature*, *352*, 397–403, doi:10.1038/352397a0.
Schoene, B., K. M. Samperton, M. P. Eddy, G. Keller, T. Adatte, S. A. Bowring, S. F. R. Khadri, and B. Gertsch (2015), U-Pb geochronology of the Deccan Traps and relation to the end-Cretaceous mass extinction, *Science*, *347*(6218), 182–184, doi:10.1126/science.aaa0118.
Schubert, G., P. Olson, C. Anderson, and P. Goldman (1989), Solitary waves in mantle plumes, *J. Geophys. Res.*, *94*(B7), 9523–9532, doi:10.1029/JB094iB07p09523.
Skilbeck, J., and J. Whitehead (1978), Formation of discrete islands in linear island chains, *Nature*, *272*, 499–501, doi:10.1038/272499a0.

Sleep, N. H. (1990), Hotspots and mantle plumes: Some phenomenology, *J. Geophys. Res.*, *95*(B5), 6715–6736, doi:10.1029/JB095iB05p06715.
Sleep, N. H. (1997), Lateral flow and ponding of starting plume material, *J. Geophys. Res.*, *102*(B5), 10,001–10,012, doi:10.1029/97JB00551.
Sleep, N. H. (2002), Ridge-crossing mantle plumes and gaps in tracks, *Geochem. Geophys. Geosyst.*, *3*(12), 8505, doi:10.1029/2001GC000290.
Sobolev, A. V., et al. (2007), The amount of recycled crust in sources of mantle-derived melts, *Science*, *316*, 412–417, doi:10.1126/science.1138113.
Sobolev, S. V., A. V. Sobolev, D. V. Kuzmin, N. A. Krivolutskaya, A. G. Petrunin, N. T. Arndt, V. A. Radko, and Y. R. Vasiliev (2011), Linking mantle plumes, large igneous provinces and environmental catastrophes, *Nature*, *477*, 312–316, doi:10.1038/nature10385.
Stein, C., and S. Stein (1992), A model for the global variation in oceanic depth and heat flow with lithospheric age, *Nature*, *359*(1), 123–129, doi:10.1038/359123a0.
Steinberger, B. (2000), Plumes in a convecting mantle: Models and observations for individual hotspots, *J. Geophys. Res.*, *105*(B5), 11,127–11,152, doi:10.1029/1999JB900398.
Steinberger, B. (2016), Topography caused by mantle density variations: Observation-based estimates and models derived from tomography and lithosphere thickness, *Geophys. J. Int.*, *205*, 604–621, doi:10.1093/gji/ggw040.
Steinberger, B., and M. Antretter (2006), Conduit diameter and buoyant rising speed of mantle plumes: Implications for the motion of hot spots and shape of plume conduits, *Geochem. Geophys. Geosyst.*, *7*, Q11018, doi:10.1029/2006GC001409.
Steinberger, B., and A. R. Calderwood (2006), Models of large-scale viscous flow in the Earth's mantle with constraints from mineral physics and surface observations, *Geophys. J. Int.*, *167*(3), 1461–1481, doi:10.1111/j.1365-246X.2006.03131.x.
Steinberger, B., and T. H. Torsvik (2012), A geodynamic model of plumes from the margins of large low shear velocity provinces, *Geochem. Geophys. Geosyst.*, *13*, Q01W09, doi:10.1029/2011GC003808.
Todal, A., and O. Eldholm (1998), Continental margin of western India and Deccan large igneous province, *Mar. Geophys. Res.*, *20*, 273–291, doi:10.1023/A:1004640508371.
Torsvik, T. H., M. A. Smethurst, K. Burke, and B. Steinberger (2006), Large igneous provinces generated from the margins of the large low-velocity provinces in the deep mantle, *Geophys. J. Int.*, *167*(3), 1447–1460, doi:10.1111/j.1365-246X.2006.03158.x.
Torsvik, T. H., B. Steinberger, M. Gurnis, and C. Gaina (2010), Plate tectonics and net lithosphere rotation over the past 150 My, *Earth Planet. Sci. Lett.*, *291*, 106–112, doi:10.1016/j.epsl.2009.12.055.
Torsvik, T. H., H. Amundsen, E. H. Hartz, F. Corfu, N. Kusznir, C. Gaina, P. V. Doubrovine, B. Steinberger, L. D. Ashwal, and B. Jamtveit (2013), A Precambrian microcontinent in the Indian Ocean, *Nat. Geosci.*, *6*(3), 223–227, doi:10.1038/ngeo1736.
Torsvik, T. H., B. Steinberger, L. D. Ashwal, P. V. Doubrovine, and R. G. Trønnes (2016), Earth evolution and dynamics—A tribute to Kevin Burke, *Can. J. Earth Sci.*, *53*(11), 1073–1087, doi:10.1139/cjes-2015-0228.
Turcotte, D. L., and G. Schubert (2002), *Geodynamics*, 2nd ed., Cambridge Univ. Press, Cambridge, U. K.
van Hinsbergen, D. J. J., B. Steinberger, P. V. Doubrovine, and R. Gassmöller (2011), Acceleration and deceleration of India-Asia convergence since the Cretaceous: Roles of mantle plumes and continental collision, *J. Geophys. Res.*, *116*, B06101, doi:10.1029/2010JB008051.

Erratum

In the originally published version of this article, supporting Figures S1–S4 were displayed separately. They have since been combined with the supporting information summary file, and this version may be considered the authoritative version of record.